RESEARCH ARTICLE

National Science Open
3: 20230073, 2024
https://doi.org/10.1360/nso/20230073

Chemistry

Rapid oxidation of black phosphorus induced by copper ions via promoting oxygen bonding and phosphate desorption

Zhiyu Zhu[1], Sha Yang[2], Kun Lu[3], Shipeng Dong[1], Xiaoyan Sun[4], Jieyin Zheng[5], Shixiang Gao[1], Wei Liu[2] & Liang Mao[1,*]

[1]*State Key Laboratory of Pollution Control and Resource Reuse, School of the Environment, Chemistry and Biomedicine Innovation Center, Nanjing University, Nanjing 210093, China;*
[2]*Nano Structural Materials Center, School of Materials Science and Engineering, Nanjing University of Science and Technology, Nanjing 210094, China;*
[3]*School of Environmental Science and Engineering, Zhejiang Gongshang University, Hangzhou 310018, China;*
[4]*Nanjing Qixia District Hospital, Nanjing 210046, China;*
[5]*Cambridge A-Level Centre, Nanjing Jinling High School, Nanjing 210005, China*

*Corresponding author (email: lmao@nju.edu.cn)

Received 25 December 2023; Revised 25 March 2024; Accepted 2 April 2024; Published online 25 April 2024

Abstract: Black phosphorus (BP) has garnered significant interest in the field of biomedicine because of its exceptional degradability. The oxidation product of BP phosphate has been utilized in numerous studies for the purpose of repairing bone defects and inducing apoptosis and autophagy in cancer cells. Nevertheless, this process has drawbacks in terms of low yield and a slow rate of phosphate production. In this study, we found that the oxidation rate of BP was increased 120-fold and the yield proportion of phosphate BP product was increased from 30% to 85% with the presence of less than 0.1% copper ions (Cu^{2+}) in the reaction system. The enhancement was attributed to the fact that the presence of Cu^{2+} promoted the bonding of oxygen on the BP surface and then the desorption of phosphate molecules from the BP surface. This study offers a novel perspective on the process of BP oxidation and introduces innovative concepts for the development of biological drug delivery systems capable of rapid decomposition.

Keywords: black phosphorus, reaction pathway, reaction efficiency, copper ions, reaction mechanism

INTRODUCTION

Nanomaterials have been extensively studied and applied to biomedicine [1–3]. Black phosphorus (BP), as a biofriendly material, is considered as a promising vehicle for anticancer drugs due to its favorable biocompatibility, strong photothermal effect, high drug loading capacity, and bioimaging capabilities [4–7]. As a kind of biomedical carrier, BP has been widely concerned and studied for its migration process *in vivo* and its stability behavior. Since BP nanosheets are linked together by monolayers of BP under van der Waals interactions, leading to their instability [8]. Currently, many studies have shown the oxidation of BP occurs in the natural environment and organisms [9,10]. At present, many studies have found that oxygen, water and light [11–13] are the main influencing factors in the oxidation of BP. Phosphate, phosphite, and hypophosphite are the major oxidation products [14–16].

© The Author(s) 2024. Published by Science Press and EDP Sciences. This is an Open Access article distributed under the terms of the Creative Commons Attribution License (https://creativecommons.org/licenses/by/4.0), which permits unrestricted use, distribution, and reproduction in any medium, provided the original work is properly cited.

Phosphate, as the oxidation product of BP, has been utilized in the treatment of bone defects [17,18] and in the induction of autophagy and apoptosis in cancer cells [19]. Nevertheless, the low yield of phosphate molecules has hindered the utilization of BP.

In addition, when BP migrates in organisms, it will contact with a variety of metal ions, such as the major metal elements sodium, magnesium, calcium and trace metal elements copper, iron and manganese [20]. However, the stability behavior of BP in contact with these metal ions is not well understood, which will make its migration and transformation behavior more complex. At present, relevant studies have found that the surface chemistry of BP will be changed when it contacts with metal, which will further affect its stability. For example, copper ions (Cu^{2+}) can specifically adsorb on the surface of BP [21], while silver ions (Ag^{+}) can bind BP through cation-Π, which enhances the stability of BP in the environment [22], which will increase its residence time and potential risk [23]. Therefore, it is necessary to investigate the stability of BP with the presence of metal ions.

Therefore, eight common metal ions in living organisms were selected in this study to investigate the stability behavior of BP in the presence of metal ions. Furthermore, Cu^{2+} was found to accelerate the oxidation of BP and enhance phosphate yield. A variety of characterization techniques and density functional theory (DFT) calculations were combined to explain the role of Cu^{2+} in the reaction.

This study offers a novel perspective on the oxidation behavior of BP and proposes a new approach to increase the yield of phosphate. Furthermore, it contributes to the advancement of the practical application of BP.

RESULTS

Characterization of Few-layered BP

The mass concentration of BP in water was measured by ultraviolet-visible (UV-vis) spectroscopy and the standard curve was displayed in Figure S1. Transmission electron microscopy (TEM) was used to characterize the morphology of the prepared BP, and it was found that the few-layered BP presented a sheet-like morphology (Figure 1a), similar to previous studies [16]. High-resolution TEM (HRTEM) image showed that the lattice spacing correlated well with 0.26 nm (Figure 1b), indicating the presence of crystalline BP, consistent with the results reported in previous studies [24]. The selective area electron diffraction (SAED) pattern of BP presented in the inset image of Figure 1b further confirmed the perfect crystalline of BP. These results demonstrated that the crystallinity of the material remained intact after being subjected to a mechanical exfoliation process in an ambient environment. Three typical bands corresponding to A^1_g, B^2_g, and A^2_g of BP at 363.1, 437.3 and 468.1 cm^{-1} were observed in the Raman spectrum, respectively (Figure 1c) [25]. The lateral size and thickness of few-layered BP were determined to be 200–1000 nm and ~1.8 nm based on the analysis of the atomic force microscopy (AFM) images (Figure 1d–f).

Cu^{2+} accelerated the oxidation of BP

BP has a negative surface charge and can bind to a variety of metal ions. Consequently, the main metal elements such as sodium (Na^{+}), magnesium (Mg^{2+}), and calcium (Ca^{2+}) and trace metals such as copper

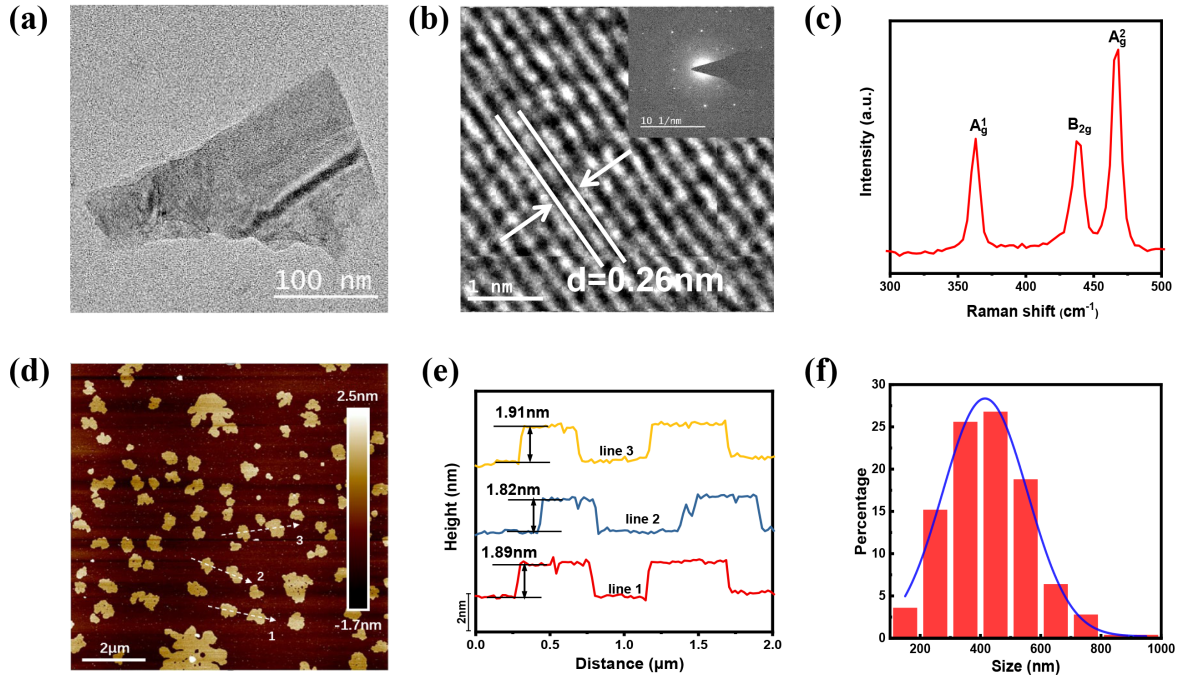


Figure 1 Characterization of the prepared BP. (a) TEM image of few-layered BP. (b) HRTEM image of BP. The inset image showed the corresponding SAED pattern. (c) Raman spectrum of BP. (d) AFM image of BP. (e) The height profiles of BP along the white lines in (c). (f) Histogram of BP size distribution. The histograms were developed by counting 200 sheets for each sample, with Gaussian fit curves shown in each histogram.

(Cu^{2+}), iron (Fe^{3+}), manganese (Mn^{2+}), zinc (Zn^{2+}), and cobalt (Co^{2+}) in human body were selected to bind with BP, and their effects on the stability of BP were studied. Figure 2a showed that 90% of BP was removed within 12 h in the presence of Cu^{2+}. In comparison, about 10%–20% of BP was oxidated in the presence of Mn^{2+}, Mg^{2+}, Ca^{2+}, Zn^{2+}, Co^{2+}, Na^{+} or Fe^{3+} in the reaction system, respectively. These findings suggest that the presence of Cu^{2+} significantly enhanced the oxidation of BP. The effect of Cu^{2+} concentrations on the oxidation rate of BP over time was further investigated. As shown in Figure 2b, the oxidation rate of BP increased with the increase of Cu^{2+} concentration. The removal of BP followed the first-order decay ($C = C_0e^{-kt}$) at the tested Cu^{2+} concentrations (Figure 2c). The pseudo-first-order kinetic constants were calculated according to fitted lines for various concentrations, which were plotted in Figure 2d. The well fitted linear regression model suggested that the oxidation of BP mediated by Cu^{2+} could be described using the second-order reaction kinetics. The second order rate constant of reaction was 0.00432 L h/μmol. The oxidation rates of BP under different concentrations (Figure S2) were also investigated.

Temperature will affect the rate of the reaction, while pH will change the zeta potential of the metal ion solution. The effects of temperature and pH on the reaction system were evaluated at different conditions, namely kept at 4, 25, 40 and 60°C, and maintaining a pH range of 3, 5, 7, 9, and 11 using an acid-base buffer solution (Figure S3). The results demonstrated that high temperatures accelerated the oxidation rate of BP, while the influence of solution pH on the reaction of BP mediated by Cu^{2+} was insignificant. In this experiment, only the effect of bare metal ions on the stability of BP was investigated, while metal ions are mostly wrapped by proteins in organisms. Therefore, ethylene diamine tetraacetic acid-Cu (EDTA-Cu) and

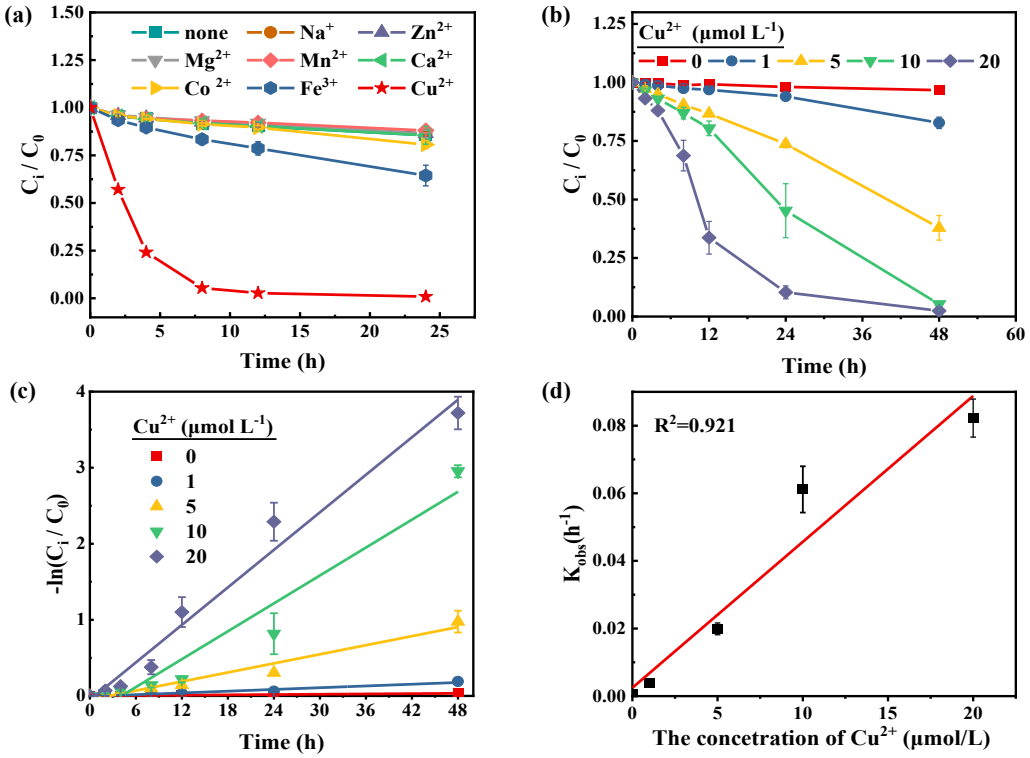


Figure 2 (a) Oxidation of BP over time with different kinds of metal ions. (b) Oxidation rates of BP at different Cu^{2+} concentrations. (c) Pseudo-first-order rate plots for oxidation of BP. (d) Relationship between pseudo-first-order rate constants and Cu^{2+} concentration. (b–d) Experimental conditions were as follows: the absorbance of BP was 0.5, [Cu^{2+}] = 1–20 μmol/L, pH = 7.0, 25°C. Error bars represent standard deviations (n = 3).

laccase (a Cu-rich protease) [26] were chosen to explore the effect of Cu^{2+} on BP in organisms and it was found that both of them can enhance the oxidation of BP (Figure S4). However, the effect of real proteins on the stability of BP and the effect of protein crowns on BP encapsulation need to be further explored [27].

Reaction products of BP

Reaction products of BP were identified in the reaction with and without the presence of Cu^{2+}, respectively. Raman spectroscopy was employed to characterize the structure changes of BP at different reaction times. The reliable A_g^1/A_g^2 ratio was used to assess the extent of BP oxidation [28]. After 2 h of reaction, the A_g^1/A_g^2 ratios decreased from 0.62 to 0.48, as observed in Figure 3a, providing evidence for the oxidation of BP in the presence of Cu^{2+}. The three characteristic peaks of BP, A_g^1, B_{2g}, and A_g^2, all showed a significant decrease of 46%, 31%, and 35%, respectively. To determine the chemical composition of the BP surface, P 2p spectra of the pristine BP and BP oxidized with Cu^{2+} for 2 h were obtained. As presented in Figure 3b, BP exhibited $2p_{3/2}$ and $2p_{1/2}$ peaks at 130.1 and 131.0 eV, respectively [29,30], which were similar to bulk BP 2p peak positions, suggesting that the structure of most BP did not undergo great change during the two-hour oxidation process. The peak at 134 eV, however, showed a substantial increase, indicating the formation of P_xO_y on the BP surface resulting from oxidation. TEM characterization revealed that during the oxidation process, the edges of BP became round, as shown in Figure 3c and d, and black spots were found to be

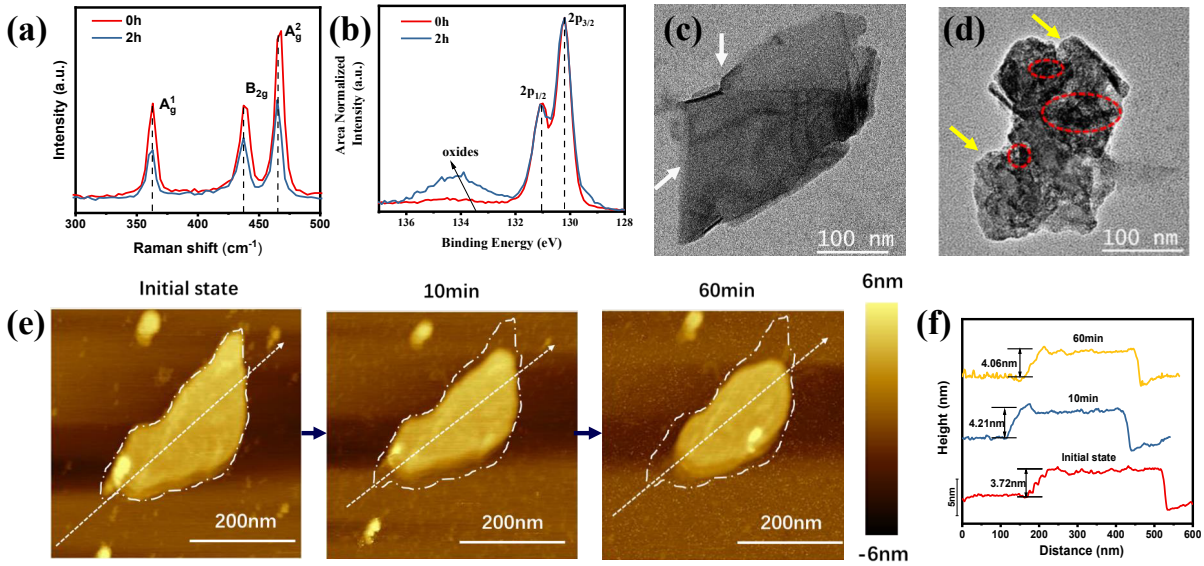


Figure 3 Characterization of BP during the reaction. (a) Raman spectra of BP in 20 μmol/L Cu^{2+} solution at 0 and 2 h. (b) XPS spectra of BP exposed to Cu^{2+}. The morphology of the BP sheet at 0 h (c) and 2 h (d) after reaction with Cu^{2+}. The white tip indicates the complete edge of the BP sheet. The yellow tip indicates the rounded edge after partial oxidation, and the red circle indicates the black spots loaded on the surface of BP. (e) *In situ* AFM images acquired with Cu^{2+} at different times, showing the morphology evolution of a BP sheet. (f) Height profiles of the BP nanoflake acquired along the dashed lines in panel (e).

attached, confirmed through energy dispersive spectrometer (EDS) analysis as copper element. *In-situ* AFM characterization was also carried out to explore the specific location of BP oxidation. The AFM measurements demonstrated that, initially, BP had an irregular edge with a thickness of approximately 4.0 nm. After the addition of Cu^{2+} for 10 min, the two ends of BP disappeared, indicating that part of BP was oxidized to P_xO_y and desorbed into the solution. The thickness of BP at the same position varied to approximately 4.2 nm due to the formation of P_xO_y adsorbed on the surface of BP. After 1 h of reaction, more parts of BP at two ends disappeared, and the edge became smooth and round. Additionally, the thickness of BP changed from approximately 4.2 nm to approximately 3.7 nm, signifying that P_xO_y also desorbed into the solution continuously. In the three-dimensional (3D) image (Figure S5), areas of increased thickness at the edge of BP were observed, corresponding to the bright spot in the 2D image, which may be interpreted as a signal of oxidation and desorption. Based on the aforementioned observations, we hypothesized that both the edge and the surface of BP were oxidized at the same time for Cu^{2+} adsorbed uniformly by BP. However, the desorption rate at the edge was obviously faster than that at the surface, which may be caused by the larger contact area of the edge with the solution.

Ion chromatography was used to identify the oxidation products of BP and three kinds of oxidation products of BP were found, namely phosphate (PO_4^{3-}), phosphorous (PO_3^{3-}), and hypophosphite (PO_2^{3-}). The standard curves for the three products are shown in Figure S6. Figure 4a showed that the concentration of PO_4^{3-}, PO_3^{3-}, and PO_2^{3-} increased by 112.2, 102.3, and 39.2 μmol/L, respectively, within 15 d. Figure 4b showed the mole fractions of PO_4^{3-} (~45 mol%), PO_3^{3-} (~40 mol%) and PO_2^{3-} (~15 mol%) in water were almost unchanged, which is consistent with Zhang's results [16]. Figure 4c showed that the concentrations of PO_3^{3-} and PO_2^{3-} had no significant change, while that of PO_4^{3-} increased significantly. At 24 h, the concentrations of PO_4^{3-}, PO_3^{3-}, and PO_2^{3-} were 223.3, 25.5, and 12.6 μmol/L, respectively. Figure 4d illustrated

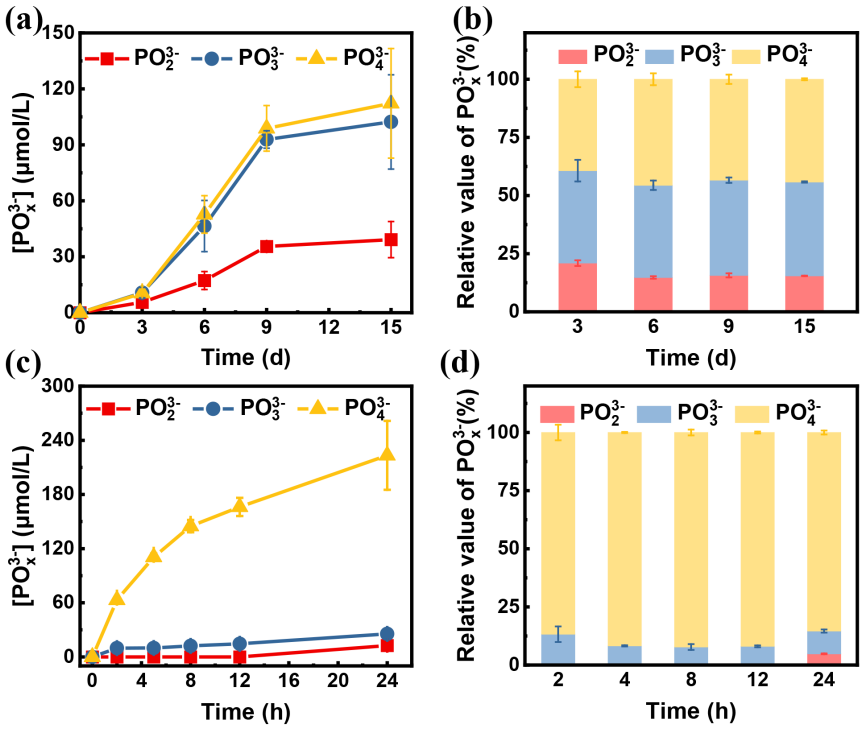


Figure 4 Relative concentrations of PO_4^{3-}, PO_3^{3-} and PO_2^{3-} compared to the values at the initial state measured by IC in the absence of Cu^{2+} (a) and in the presence of Cu^{2+} (c). Mole fractions of PO_4^{3-}, PO_3^{3-}, and PO_2^{3-} were measured at different storage times in the absence of Cu^{2+} (b) and in the presence of Cu^{2+} (d).

that >85% of the reaction products were PO_4^{3-} for the reaction of BP with Cu^{2+}. The fraction alteration of the oxidation products of BP revealed that the participation of Cu^{2+} changed the reaction pathway.

Reaction pathway and possible mechanisms

The oxidation process of BP in air is predominantly controlled by the presence of oxygen, water, and light [11–13], thus the impact of each of these components on the BP-Cu^{2+} reaction system was examined. Our experimental findings suggest that, while light had a negligible effect on the reaction system, water and oxygen were indispensable components of the reaction, as demonstrated in Figure S7. At the same time, reactive oxygen species are considered to be important factors affecting the oxidation of BP [31]. Therefore, quenching agents including hydroxyl radical, singlet oxygen and superoxide anion are selected to evaluate the possible participation of reactive oxygen in the reaction. As shown in Figure S8, the effect of reactive oxygen species is almost negligible in the current experiment.

Drawing upon the aforementioned results and available literature on Cu^{2+} as mediators, we postulated that the BP-Cu^{2+} reaction system can be conceptualized to comprise three distinct processes (Figure 5): (i) the enhanced adsorption and bonding of oxygen to the BP-Cu^{2+} surface, triggered by the presence of Cu^{2+}; (ii) the oxidation of the BP surface layer into three kinds of phosphate groups and the simultaneous reduction of Cu^{2+} to cuprous ions; (iii) the release of the phosphate groups into the solution and the subsequent dissolution of cuprous ions from the BP surface. While the above three steps are carried out, the shed cuprous ions are

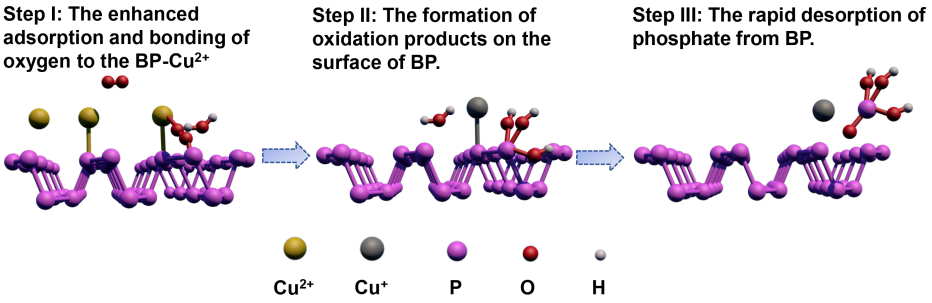


Figure 5 The mechanism of rapid oxidation of BP in the presence of Cu^{2+}.

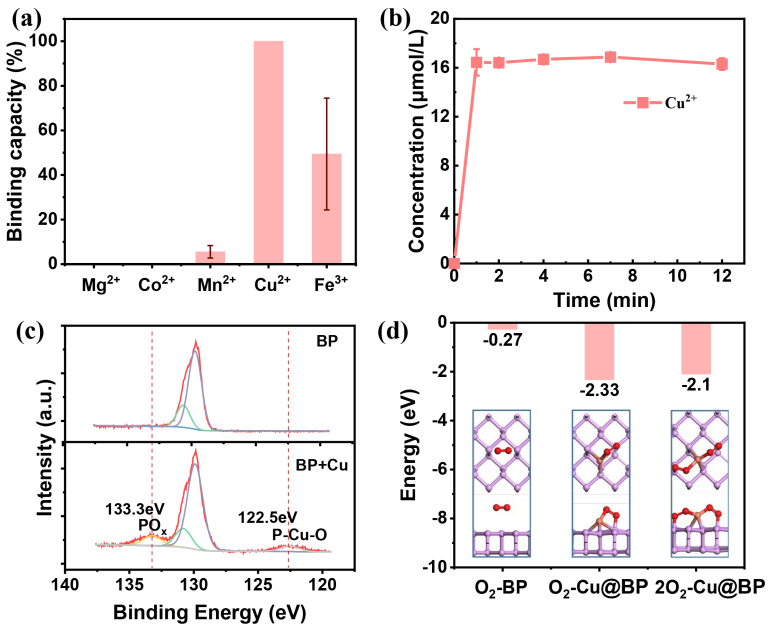


Figure 6 (a) Bind capacity of BP nanosheets to different metal ions. (b) Adsorption kinetics curve of BP on the Cu^{2+}. (c) XPS spectra of BP nanosheets before and after Cu adsorption for 1 h. (d) Schematic diagram of oxygen molecule adsorption on the surface of BP before and after Cu adsorption.

oxidized to Cu^{2+} by the ambient oxygen, and continue to participate in the reaction.

In step I, Cu^{2+} was quickly adsorbed onto the BP surface at first, and then oxygen molecules were adsorbed between Cu^{2+} and BP to form chemical bonds. To corroborate the hypothesis of rapid Cu^{2+} adsorption onto the BP surface, a series of adsorption experiments involving various ions on the BP surface were conducted. As depicted in Figure 6a, nearly all of the added Cu^{2+} were rapidly absorbed by the BP, while the adsorption capacity of the BP for iron ions was limited to approximately 50%, which was consistent with the adsorption results in other studies [21]. The adsorption rate of various other tested metal ions was also markedly lower than that of Cu^{2+}, thereby corroborating the promotion performance of BP observed in Figure 2A. Moreover, to determine the adsorption time of Cu^{2+} on BP, experiments were conducted for varying adsorption periods. In order to explore the adsorption time between BP and Cu^{2+}, adsorption experiments were performed at different time points. Figure 6b manifested that Cu^{2+} was adsorbed within 1 min on the BP surface. Nevertheless, a more meticulous investigation is warranted to discern the precise adsorption time between

BP and Cu^{2+}.

To verify that Cu^{2+} could enhance the adsorption capacity of BP to oxygen molecules, X-ray photoelectron (XPS) and DFT calculations were performed. The XPS spectra revealed the emergence of a new peak in the range from 122 to 124 eV in the BP-Cu^{2+} group that was absent in the control group (Figure 6c). Preliminary inspection by the National Institute of Standards and Technology (NIST) suggested that this peak may be linked to the P–Cu–O bond, a finding not previously reported in the literature. To further validate this observation, DFT calculations were conducted to gauge the energy required for oxygen adsorption on the BP surface, with or without the presence of Cu^{2+}. As depicted in Figure 6d, the energy required for oxygen molecule adsorption onto the pure BP surface was −0.27 eV, while this value plummeted to −2.33 eV in the presence of Cu^{2+}. Moreover, upon the addition of another oxygen molecule to the model, the binding was still intact, and the required energy (−2.1 eV) remained considerably lower than that observed without the intervention of Cu^{2+}. Similar DFT calculations (Figure S9) performed at the BP edge equally supported our hypothesis that Cu^{2+} facilitated oxygen binding on the BP.

In step II, Cu^{2+} mediated the oxidation of BP into three distinct phosphoric acid products. There are two widely accepted views on the oxidation of BP without Cu^{2+}. First of all, water molecules are known to pluck the surface oxides of BP in the course of their oxidation, owing to hydrogen bonding [30]. In addition, Zhang's research [16] identified three distinct oxidation products of BP. However, in contrast to extant studies, the addition of Cu^{2+} exerted a discernable impact on the formation and desorption energies of these phosphoric acid molecules, leading to modifications in their actual formation ratios. The formation energies of the three phosphoric acid molecules on pure BP and BP-Cu^{2+} complexes were calculated using DFT. As illustrated in Figure 7a, the formation energies of H_3PO_2, H_3PO_3, and H_3PO_4 on the pure BP surface were computed to be −1.96, −3.81, and −6.89 eV, respectively. By contrast, on the BP-Cu^{2+} complex surface (Figure 7b), these energy values were found to be −4.62, −7.03, and −9.83 eV, respectively. These calculation results showed that in the presence of Cu^{2+}, the formation energy of the three phosphate molecules decreases, indicating that they were generated faster than before, which leads to a faster oxidation rate of BP. This result was consistent with the results in Figure 2a.

At the same time, Cu^{2+} would be reduced to cuprous ions, and XPS was carried out to prove it. Figure S10A showed that Cu^{2+} mainly existed in the form of copper monovalent. Also, we tried to use monovalent copper ions to accelerate the oxidation of BP, and found that the promoting effect of cuprous ions was the same as that of copper ions (Figure S10B).

In step III, the three kinds of phosphate moieties overcame the adsorption energy barrier and desorbed from the surface of BP. The desorption energies of the three phosphoric acid molecules at both pure BP and BP-Cu^{2+} complexes were calculated via DFT. As displayed in Figure 7c, the desorption energies of H_3PO_2, H_3PO_3, and H_3PO_4 on pure BP surfaces were 0.93, 0, and 0.66 eV, respectively. While the phosphoric acid molecule exhibited a lower formation energy (−6.89 eV), a desorption energy of 0.66 eV was required. By comparison, the formation energy for the phosphite molecule (−3.81 eV) did not necessitate any additional energy for its detachment, and hence the highest proportion of phosphite was found in the oxidation products of BP, which was consistent with the results of Figure 4b. In the presence of Cu^{2+}, the desorption energies of the three phosphoric acid molecules were increased to 1.39, 1.41, and 1.24 eV, respectively. Thereby, the calculation results showed that the desorption energy of phosphate molecule was the lowest among the three, and its formation energy was the lowest at 9.83 eV, implying that the proportion of phosphate molecule in the

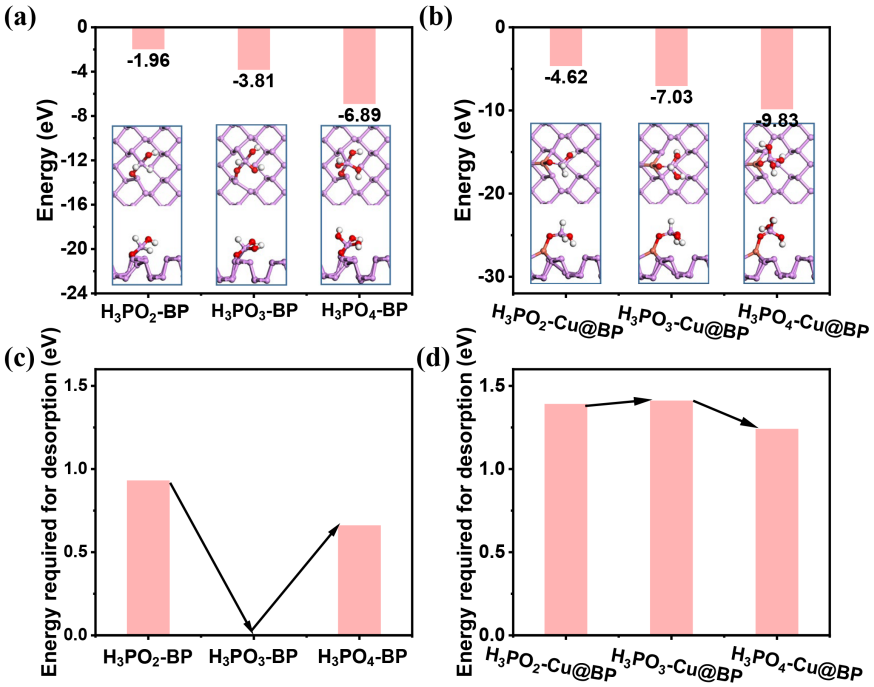


Figure 7 (a) Structure of the formed H_3PO_x and the corresponding formation energies for pristine BP. (b) Structure of the formed H_3PO_x and the corresponding formation energies for Cu@BP. (c) Desorption barrier of H_3PO_x from BP calculated by CI-NEB method. (d) Desorption barrier of H_3PO_x from Cu@BP calculated by CI-NEB method.

oxidation product of BP was the highest, which was consistent with the results in Figure 4d. As the three phosphoric acid molecules detached and were shed from the BP surface, additional defect sites became exposed, thus facilitating subsequent reactions.

CONCLUSION

In summary, we found that the presence of Cu^{2+} accelerated the oxidation process of BP. The enhancement was attributed to the fact that the presence of Cu^{2+} promoted the bonding of oxygen on the BP surface and then the desorption of phosphate molecules from the BP surface. The Cu^{2+} themselves undergo dynamic changes during the reaction. Our results improve the understanding of BP oxidation and provide new ideas for the application of BP in stability studies and drug nanocarrior ablation studies.

MATERIALS AND METHODS

Materials

BP crystals were acquired from XFNANO Materials Tech Co., Ltd. in Nanjing, China, and subsequently transferred into a brown bottle within an argon-filled glove box. Additional chemicals were procured from Aladdin Biochemical Technology Co., Ltd. (Shanghai, China) or Sigma-Aldrich (St. Louis, MI, USA)

through commercial channels. All reagents used in the experiment were of analytical grade.

Preparation of few-layer BP

BP crystals weighing 30 mg were pulverized and dispersed in 100 mL of deoxygenated ultra-pure water. The solution was subjected to sonication using a pin sonicator for 20 h at 90 W. Subsequently, the brown suspension was centrifuged at 3000 r/min for 10 min to eliminate bulk BP, and the resulting supernatant was retained for subsequent analysis.

Characterization of BP

The morphology and size of BP were analyzed using TEM (FEI Tecnai F20, USA) with a molybdenum network as the substrate and AFM (Bruker USA) with a mica sheet as the substrate. The hydrodynamic size distribution of BP was determined using a Zetasizer (Nano ZS, Britain). The Raman spectra were acquired using a Raman spectrometer (LabRam HR Evolution) with 532 nm laser excitation.

Assessment of oxidation of BP at different conditions

The experiments were conducted in 8 mL centrifuge-tube batch reactors that were vibrated on a rotary shaker operating at 100 r/min. A 3-mL reaction solution was prepared in ultrapure water containing a BP suspension with an absorbance of 0.5, and 20 μmol/L of metal ions, including Mn^{2+}, Mg^{2+}, Ca^{2+}, Zn^{2+}, Co^{2+}, Na^{2+}, Fe^{3+}, and Cu^{2+}. Subsequently, metal ions were introduced into each reactor to commence the reaction. Controls were established by utilizing a reactor that was identical but lacked metal ions. The solution was sampled at specified time intervals (0, 2, 4, 8, 12, and 24 h) and promptly analyzed using the UV-vis absorption spectrometer (UV-5000) for measurement. The suspension underwent sonication prior to UV-vis measurements in order to minimize the impact of flake-restacking during the measurement.

Experiments were carried out using an identical reactor device and procedure as previously outlined to examine the influence of temperature and pH on the oxidation of BP facilitated by metal ions. The temperature gradient was established at 4, 25, 40, and 60°C. Buffer solutions with pH values of 3, 5, 7, 9, and 11 were employed to investigate the impact of pH on the BP-Cu system, replacing the initial water. Following the experiment, the pH of the solution was re-measured.

Characterization of BP during oxidation

Raman spectroscopy was employed to analyze the freshly prepared BP following a 2-h reaction with Cu^{2+}. The X-ray photoelectron spectroscopy (XPS) spectrum was obtained using an X-ray photoelectron spectroscopy instrument from Thermo Fischer, USA. The BP suspension was deposited onto the filter paper of a vacuum suction filtration system and subsequently stored in a glove box prior to XPS characterization, with varying reaction times. During the XPS test, the sweep parameter was set to 10 with a step of 0.1. The TEM (FEI Tecnai F20, USA) was employed to examine the morphology of BP in a Cu^{2+} solution at 0 and 2 h. Additionally, EDS-mapping analysis was conducted to differentiate the chemical element content on the

surface of BP during the reaction. The oxidation behavior of BP under the influence of Cu^{2+} was characterized using *in situ* AFM (Cyper ES, Asylum Research) with the BL-AC40TS probe model (Olympus). The probes underwent calibration for elastic modulus in air and sensitivity in the liquid environment prior to characterization. Subsequently, the BP was deposited onto the surface of the freshly peeled mica sheet. Following the absorption of BP, the mica sheet's surface was rinsed with ultrapure water, and subsequently, 100 μL of water was added to establish a liquid environment. The light tapping technique was employed to scan the surface of BP in order to identify an appropriate sample for use as a control. A 1-mL syringe was attached to the submerged perfusion holder, and the water on BP was substituted with a Cu^{2+} solution. The procedure was conducted thrice using a liquid injection volume of 100 μL. BP was monitored for a duration of 1 h following readjustment of the laser.

Characterization of the oxidation products of BP

The experiments were conducted in 8 mL centrifuge-tube batch reactors that were vibrated on a rotary shaker operating at 100 r/min. A 3-mL reaction solution was prepared in ultrapure water containing a BP suspension with an absorbance of 0.5 and 20 mmol Cu^{2+}. At specified time points (0, 2, 4, 8, 12, and 24 h), the solution was drawn into a 1-mL syringe and subsequently filtered through a 0.22-μm needle filter to eliminate the incompletely oxidized BP sheet. The filtrate was collected for subsequent analysis of anion form and content using ion chromatography (ICS-5000, Thermo, USA). The experiments utilized a 30 mmol/L KOH solution as the eluent. The control group was established without Cu^{2+} in the BP solution. In order to ensure that the oxidation products were within the detectable range, the oxidation time of BP was extended due to the slow oxidation rate of the system. Consequently, the sampling intervals for BP oxidation in the absence of Cu^{2+} were established at 0, 3, 6, and 9 days.

Computational methods

The DFT calculations were conducted using the Vienna *Ab initio* Simulation Package (VASP) [32,33]. The optB88-vdW functional [34] was utilized to incorporate the van der Waals forces. The formation energy of H_3PO_x can be determined through calculation as described in reference [16].

The chemical equation can be represented as follows:

$$\mathrm{BP} + a\mathrm{OH} + b\ \mathrm{H} + c\ \mathrm{O} = \mathrm{BP\text{-}H_3PO}_x\ (x = 2, 3, 4),$$
$$a = 2,\ b = 1,\ c = 0,\ \text{and}\ x = 2;$$
$$a = 3,\ b = 0,\ c = 0,\ \text{and}\ x = 3;$$
$$a = 3,\ b = 0,\ c = 1,\ \text{and}\ x = 2.$$

The climbing image nudged elastic band (CI-NEB) method was employed to determine the activation barrier for desorption from the BP and Cu-doped BP substrate [35]. Five images were included between the initial and final state in order to investigate the transition state. The structure was optimized iteratively until the magnitude of the force acting on each atom was reduced to less than 0.05 eV/Å. The two-dimensional Brillouin zone was sampled using a 5 × 6 × 1 mesh, following the Monkhorst-Pack method [36]. The BP slab was simulated using a 3 × 2 supercell. In order to prevent interlayer interaction, a vacuum of more than 10 Å was introduced between the slabs.

Data analysis

Each experiment was conducted three times under each condition, and the reported values represent the means ± standard deviation of the three parallel experiments. All statistical analyses were conducted using Statistical Packages for the Social Sciences (SPSS) Version 19.03.

Data availability

The original data are available from corresponding authors upon reasonable request.

Acknowledgements

The authors are grateful to the editors and the anonymous reviewers for their insightful comments and suggestions.

Funding

This work was supported by the National Natural Science Foundation of China (22125602, U2067215, 22206087 and 22076078) and the National Key R&D Program of China (2022YFC3701402).

Author contributions

Z.Z. performed the experiments. Z.Z. and L.M. conceived the project and contributed to the design of the experiments and analysis of the data. S.Y. and W.L. performed the DFT calculations. All the authors discussed the results and commented on the manuscript.

Conflict of interest

The authors declare no conflict of interest.

Supplementary information

The supporting information is available online at https://doi.org/10.1360/nso/20230073. The supporting materials are published as submitted, without typesetting or editing. The responsibility for scientific accuracy and content remains entirely with the authors.

References

1 Zheng F, Chen Z, Li J, *et al.* A highly sensitive crispr-empowered surface plasmon resonance sensor for diagnosis of inherited diseases with femtomolar-level real-time quantification. *Adv Sci* 2022; **9**: e2105231.

2 Chen Z, Wu C, Yuan Y, *et al.* CRISPR-Cas13a-powered electrochemical biosensor for the detection of the L452R mutation in clinical samples of SARS-CoV-2 variants. *J Nanobiotechnol* 2023; **21**: 141.

3 Chen Z, Li J, Li T, *et al.* A CRISPR/Cas12a-empowered surface plasmon resonance platform for rapid and specific diagnosis of the Omicron variant of SARS-CoV-2. *Natl Sci Rev* 2022; **9**: nwac104.

4 Qu G, Xia T, Zhou W, *et al.* Property-activity relationship of black phosphorus at the nano-bio interface: From molecules to organisms. *Chem Rev* 2020; **120**: 2288–2346.

5 Tao W, Zhu X, Yu X, *et al.* Black phosphorus nanosheets as a robust delivery platform for cancer theranostics. *Adv Mater* 2017; **29**: 1603276.

6 Yang B, Yin J, Chen Y, *et al.* 2D-black-phosphorus-reinforced 3D-printed scaffolds: A stepwise countermeasure for osteosarcoma. *Adv Mater* 2018; **30**: 1705611.

7 Shao J, Xie H, Huang H, *et al.* Biodegradable black phosphorus-based nanospheres for *in vivo* photothermal cancer

therapy. *Nat Commun* 2016; **7**: 12967.

8 Wild S, Fickert M, Mitrovic A, *et al.* Lattice opening upon bulk reductive covalent functionalization of black phosphorus. *Angew Chem Int Ed* 2019; **58**: 5763–5768.

9 van Druenen M. Degradation of black phosphorus and strategies to enhance its ambient lifetime. *Adv Mater Inter* 2020; **7**: 2001102.

10 Peng L, Abbasi N, Xiao Y, *et al.* Black phosphorus: Degradation mechanism, passivation method, and application for *in situ* tissue regeneration. *Adv Mater Inter* 2020; **7**: 2001538.

11 Niu X, Li Y, Zhang Y, *et al.* Photo-oxidative degradation and protection mechanism of black phosphorus: Insights from ultrafast dynamics. *J Phys Chem Lett* 2018; **9**: 5034–5039.

12 Zhou Q, Chen Q, Tong Y, *et al.* Light-induced ambient degradation of few-layer black phosphorus: mechanism and protection. *Angew Chem Int Ed* 2016; **55**: 11437–11441.

13 Zhang S, Zhang X, Lei L, *et al.* Ph-dependent degradation of layered black phosphorus: Essential role of hydroxide ions. *Angew Chem Int Ed* 2019; **58**: 467–471.

14 Plutnar J, Sofer Z, Pumera M. Products of degradation of black phosphorus in protic solvents. *ACS Nano* 2018; **12**: 8390–8396.

15 Wang Y, Yang B, Wan B, *et al.* Degradation of black phosphorus: A real-time ^{31}P NMR study. *2D Mater* 2016; **3**: 035025.

16 Zhang T, Wan Y, Xie H, *et al.* Degradation chemistry and stabilization of exfoliated few-layer black phosphorus in water. *J Am Chem Soc* 2018; **140**: 7561–7567.

17 Long J, Yao Z, Zhang W, *et al.* Regulation of osteoimmune microenvironment and osteogenesis by 3D-printed PLAG/black phosphorus scaffolds for bone regeneration. *Adv Sci* 2023; **10**: 2302539.

18 Xu Y, Mo J, Wei W, *et al.* Oxidized black phosphorus nanosheets as an inorganic antiresorptive agent. *CCS Chem* 2021; **3**: 1105–1115.

19 Li Y, Fang Q, Sheng JYH, *et al.* Cancer cell-specific autophagy activation using phosphorus-based nanoplatform as anabolism activator. *ACS Mater Lett* 2023; **5**: 2028–2038.

20 Zoroddu MA, Aaseth J, Crisponi G, *et al.* The essential metals for humans: A brief overview. *J Inorg Biochem* 2019; **195**: 120–129.

21 Chen W, Ouyang J, Yi X, *et al.* Black phosphorus nanosheets as a neuroprotective nanomedicine for neurodegenerative disorder therapy. *Adv Mater* 2018; **30**: 1703458.

22 Guo Z, Chen S, Wang Z, *et al.* Metal-ion-modified black phosphorus with enhanced stability and transistor performance. *Adv Mater* 2017; **29**: 1703811.

23 Shao X, Ding Z, Zhou W, *et al.* Intrinsic bioactivity of black phosphorus nanomaterials on mitotic centrosome destabilization through suppression of PLK1 kinase. *Nat Nanotechnol* 2021; **16**: 1150–1160.

24 Ahmed T, Balendhran S, Karim MN, *et al.* Degradation of black phosphorus is contingent on UV-blue light exposure. *npj 2D Mater Appl* 2017; **1**: 18.

25 Favron A, Gaufrès E, Fossard F, *et al.* Photooxidation and quantum confinement effects in exfoliated black phosphorus. *Nat Mater* 2015; **14**: 826–832.

26 Khatami SH, Vakili O, Movahedpour A, *et al.* Laccase: Various types and applications. *Biotech App Biochem* 2022; **69**: 2658–2672.

27 Mo J, Xie Q, Wei W, *et al.* Revealing the immune perturbation of black phosphorus nanomaterials to macrophages by understanding the protein corona. *Nat Commun* 2018; **9**: 2480.

28 Alsaffar F, Alodan S, Alrasheed A, *et al.* Raman sensitive degradation and etching dynamics of exfoliated black phosphorus. *Sci Rep* 2017; **7**: 44540.

29 Wu S, He F, Xie G, *et al.* Black phosphorus: Degradation favors lubrication. *Nano Lett* 2018; **18**: 5618–5627.

30 van Druenen M, Davitt F, Collins T, *et al.* Evaluating the surface chemistry of black phosphorus during ambient degradation. *Langmuir* 2019; **35**: 2172–2178.

31 Wang H, Yang X, Shao W, *et al.* Ultrathin black phosphorus nanosheets for efficient singlet oxygen generation. *J Am Chem Soc* 2015; **137**: 11376–11382.

32 Kresse G, Furthmüller J. Efficiency of ab-initio total energy calculations for metals and semiconductors using a plane-wave basis set. *Comput Mater Sci* 1996; **6**: 15–50.

33 Kresse G, Furthmüller J. Efficient iterative schemes for *ab initio* total-energy calculations using a plane-wave basis set. *Phys Rev B* 1996; **54**: 11169–11186.

34 Klimeš J, Bowler DR, Michaelides A. Chemical accuracy for the van der Waals density functional. *J Phys-Condens Matter* 2010; **22**: 022201.

35 Henkelman G, Uberuaga BP, Jónsson H. A climbing image nudged elastic band method for finding saddle points and minimum energy paths. *J Chem Phys* 2000; **113**: 9901–9904.

36 Monkhorst HJ, Pack JD. Special points for Brillouin-zone integrations. *Phys Rev B* 1976; **13**: 5188–5192.